

# Large nitric acid trihydrate particles and denitrification caused by mountain waves in the Arctic stratosphere

G. W. Mann, K. S. Carslaw, M. P. Chipperfield, and S. Davies

Institute for Atmospheric Science, School of the Environment, University of Leeds, Leeds, UK

S. D. Eckermann

Middle Atmospheric Dynamics Section, E. O. Hulburt Center for Space Research, Naval Research Laboratory, Washington, D. C., USA

Received 23 July 2004; revised 12 November 2004; accepted 17 December 2004; published 20 April 2005.

[1] The contribution of stratospheric mountain waves to the formation of large nitric acid trihydrate (NAT) particles and subsequent denitrification of the Arctic polar vortex is calculated for the 1999/2000 winter using a three-dimensional (3-D) model. The model production mechanism involves the formation of NAT clouds with high particle number concentrations downwind of mountain wave ice clouds, as has been previously observed. These wave-induced NAT clouds then serve as “mother clouds” for the release of low concentrations of sedimenting NAT particles, following the mechanism of Fueglistaler et al. (2002a). Our calculations show that wave-induced NAT mother clouds can occupy up to 5–10% of the volume of air below the NAT temperature. NAT particles that have sedimented from the mother cloud bases can occupy in excess of 60% of the NAT supersaturated region. Integrated over the entire vortex at the end of the 1999/2000 simulation, it is estimated that denitrification due to this mechanism could potentially be responsible for as much as 80% of that observed. These results show that mountain waves may contribute to the occurrence of solid polar stratospheric clouds more than was previously thought and that they may play a significant role in denitrification.

**Citation:** Mann, G. W., K. S. Carslaw, M. P. Chipperfield, S. Davies, and S. D. Eckermann (2005), Large nitric acid trihydrate particles and denitrification caused by mountain waves in the Arctic stratosphere, *J. Geophys. Res.*, *110*, D08202, doi:10.1029/2004JD005271.

## 1. Introduction

[2] Chemical destruction of polar stratospheric ozone can be prolonged significantly by the sedimentation of nitric acid-containing polar stratospheric cloud (PSC) particles. In several recent Arctic winters denitrification has been observed over large areas despite synoptic-scale temperatures rarely falling below the ice frost point [e.g., Waibel et al., 1999; Kondo et al., 2000; Santee et al., 2000; Popp et al., 2001].

[3] In the 1999/2000 Arctic winter, the NO<sub>y</sub> instrument aboard the ER-2 aircraft [Fahey et al., 2001] measured widespread large (up to 20 μm diameter) nitric acid-containing particles (assumed to be nitric acid trihydrate) at low number densities (10<sup>-5</sup> to 10<sup>-3</sup> cm<sup>-3</sup>). Carslaw et al. [2002] and Drdla et al. [2002] showed that the meteorology in that winter was such that NAT particles could grow to these sizes. Mann et al. [2002] used the 3-D denitrification by Lagrangian particle sedimentation (DLAPSE) model to demonstrate that NAT particles with such low concentrations could cause significant denitrification in four recent

cold Arctic winters. A thorough evaluation of the DLAPSE model has been carried out by Davies et al. [2005] against a wealth of denitrification observations. The model captures the observed timing, magnitude and extent of denitrification for the 1999/2000 and 1996/1997 winters very well, although it slightly underestimates the magnitude of denitrification in the 1994/1995 winter.

[4] In each of the DLAPSE model studies above, a relatively simple nucleation mechanism was assumed in which particles are nucleated at a constant volume average rate wherever the temperatures are below the NAT equilibrium temperature (around 195 K). This simple “large-scale” nucleation mechanism was used because it was the most straightforward way to produce geographically widespread low concentrations of NAT as observed [Northway et al., 2002; Fahey et al., 2001]. Despite the success of the DLAPSE model in broadly reproducing denitrification using this simple nucleation mechanism, the real mechanism for the production of widespread low concentrations of NAT particles remains uncertain. A mechanism involving synoptic-scale ice-induced NAT was shown by Carslaw et al. [2002] not to produce NAT over areas as large as observed. Furthermore, rates of homogeneous freezing nucleation of NAT from ternary solution droplets dependent

## Report Documentation Page

*Form Approved*  
*OMB No. 0704-0188*

Public reporting burden for the collection of information is estimated to average 1 hour per response, including the time for reviewing instructions, searching existing data sources, gathering and maintaining the data needed, and completing and reviewing the collection of information. Send comments regarding this burden estimate or any other aspect of this collection of information, including suggestions for reducing this burden, to Washington Headquarters Services, Directorate for Information Operations and Reports, 1215 Jefferson Davis Highway, Suite 1204, Arlington VA 22202-4302. Respondents should be aware that notwithstanding any other provision of law, no person shall be subject to a penalty for failing to comply with a collection of information if it does not display a currently valid OMB control number.

1. REPORT DATE <b>12 NOV 2004</b>	2. REPORT TYPE	3. DATES COVERED <b>00-00-2004 to 00-00-2004</b>			
4. TITLE AND SUBTITLE <b>Large nitric acid trihydrate particles and denitrification caused by mountain waves in the Arctic stratosphere</b>		5a. CONTRACT NUMBER			
		5b. GRANT NUMBER			
		5c. PROGRAM ELEMENT NUMBER			
6. AUTHOR(S)		5d. PROJECT NUMBER			
		5e. TASK NUMBER			
		5f. WORK UNIT NUMBER			
7. PERFORMING ORGANIZATION NAME(S) AND ADDRESS(ES) <b>Naval Research Laboratory, E.O. Hulburt Center for Space Research, Washington, DC, 20375</b>		8. PERFORMING ORGANIZATION REPORT NUMBER			
9. SPONSORING/MONITORING AGENCY NAME(S) AND ADDRESS(ES)		10. SPONSOR/MONITOR'S ACRONYM(S)			
		11. SPONSOR/MONITOR'S REPORT NUMBER(S)			
12. DISTRIBUTION/AVAILABILITY STATEMENT <b>Approved for public release; distribution unlimited</b>					
13. SUPPLEMENTARY NOTES					
14. ABSTRACT					
15. SUBJECT TERMS					
16. SECURITY CLASSIFICATION OF:			17. LIMITATION OF ABSTRACT	18. NUMBER OF PAGES	19a. NAME OF RESPONSIBLE PERSON
a. REPORT <b>unclassified</b>	b. ABSTRACT <b>unclassified</b>	c. THIS PAGE <b>unclassified</b>	<b>Same as Report (SAR)</b>	<b>12</b>	

on temperature and NAT supersaturation appear to be too low under stratospheric conditions [Knopf *et al.*, 2002], although there is some dispute about how laboratory experiments should be interpreted [Tabazadeh, 2003].

[5] The only proposed NAT formation mechanism that has been observed and successfully modelled is that involving mountain wave-induced ice clouds. Numerous observations show that NAT exists downwind of such clouds [Carslaw *et al.*, 1998; Wirth *et al.*, 1999; Hu *et al.*, 2002; Fueglistaler *et al.*, 2002b; Voigt *et al.*, 2003; Luo *et al.*, 2003]. These studies have combined detailed meteorological, microphysical and optical models to derive properties of NAT and ice clouds that are in very good agreement with aircraft and balloon observations. All of these studies show that NAT is most likely nucleated on ice particles in the wave clouds to produce fairly high NAT concentrations downwind. Carslaw *et al.* [1999] showed using a mountain wave parameterization that the sum of mountain waves in the Arctic could produce widespread NAT clouds in the vortex. Given the expected high concentrations and small sizes of the particles in these mountain wave-induced clouds, their influence on denitrification was not explored. Although geographically widespread, the NAT clouds were only predicted to cover around 5% of the NAT supersaturated region for this 1994/1995 winter at maximum. In contrast, subsequent analyses of ground-based [Biele *et al.*, 2001] and airborne [Toon *et al.*, 2000] lidar measurements have inferred that solid PSCs have a much wider coverage.

[6] More recently, Fueglistaler *et al.* [2002a] and Dhaniyala *et al.* [2002] have suggested that PSCs with high concentrations and small sizes of NAT become very extended in the vertical because of sedimentation, and ultimately cause denitrification. Fueglistaler *et al.* [2002a] termed such clouds “mother clouds” and showed using a column model that they could produce low concentrations of large NAT particles (5–10  $\mu\text{m}$  radius) several kilometers below the mother cloud after about 5 days, a prediction that has some observational support [Fueglistaler *et al.*, 2002b]. Mountain waves are one possible source of mother clouds.

[7] In this study we use the 3-D DLAPSE model to investigate how effective mountain waves could be in producing widespread low concentrations of large NAT particles by the mother-cloud mechanism. We then go on to calculate how much of the observed denitrification in the 1999/2000 Arctic winter cloud have been caused by these large NAT particles. These calculations are compared with a model run using the “large-scale” constant volume average nucleation mechanism, which has been shown to capture the timing and extent of a wide range of observations of denitrification in several recent cold Arctic winters [Davies *et al.*, 2005].

## 2. Methodology

### 2.1. Description of the DLAPSE Model

[8] The DLAPSE model is described fully by Carslaw *et al.* [2002] and Mann *et al.* [2002]. Briefly, the model consists of a Lagrangian particle model incorporating the formation, advection, growth and sedimentation of several thousand NAT particles coupled to the 3-D Eulerian off-line stratospheric chemical transport model (CTM) SLIMCAT [e.g., Chipperfield, 1999]. The DLAPSE module calculates the

change in gas phase  $\text{HNO}_3$  concentration in each SLIMCAT grid box caused by particle growth (and evaporation), advection and sedimentation in each time step. Supercooled ternary solution (STS) droplet formation in the model is calculated according to Carslaw *et al.* [1995] and has the effect of reducing the rate of NAT particle growth in very cold regions. The Eulerian CTM produces fields of denitrification calculated as the difference between the total  $\text{HNO}_3$  (in the gas, solid and liquid phases) and a passive  $\text{HNO}_3$  tracer with the feedback on NAT growth switched off. The 3-D Lagrangian particle advection and the Eulerian trace gas advection are both done with a time step of 30 min.

[9] The model is forced by 6-hour wind and temperature fields from operational analyses of the European Centre for Medium-Range Weather Forecasts (ECMWF), while vertical tracer advection is calculated in isentropic coordinates from heating rates using the MIDRAD radiation scheme [Shine, 1987]. For all the simulations in this paper, the CTM has  $1^\circ \times 1^\circ$  horizontal resolution with a 10 K vertical resolution between 350 and 600 K and 30 K resolution between 600 and 690 K. The horizontal resolution is much finer than used in previous DLAPSE simulations in order to capture the finer-scale NAT clouds downwind of mountain waves (and to be compatible with the mountain wave model output).

[10] When used for “full chemistry” denitrification studies (such as that of Davies *et al.* [2005]), the CTM is run with a 41-tracer chemistry scheme. However, to reduce computation time in these high-resolution simulations, a reduced four-tracer scheme was used as also used by Carslaw *et al.* [2002], Mann *et al.* [2002] and Mann *et al.* [2003]. The four tracers are  $\text{NO}_y$ , passive  $\text{NO}_3$ ,  $\text{H}_2\text{O}$  and aerosol  $\text{H}_2\text{SO}_4$  (required for the STS calculation). This four-tracer scheme enables the effect of the microphysics on fields of  $\text{NO}_y$  to be examined without including the full chemistry. For this scheme, an assumption is made that all  $\text{NO}_y$  is in the form of  $\text{HNO}_3$ , which is reasonable for the winter lower polar stratosphere. The chemical tracers are advected using the second-order moments scheme of Prather [1986], which has low numerical diffusion and performs well in preserving strong gradients that often arise during strong denitrification.

[11] For the simulations in this paper, the coupled model is initialized on 1 December 1999 at 1200 UT using 3-D fields of gas phase nitric acid and water from a multiannual SLIMCAT simulation. These compare reasonably well with observations from 1999/2000 below 700 K [Davies, 2003].

### 2.2. Mountain Wave Model

[12] We use global grid-averaged fields of peak mountain wave temperature perturbations derived from daily hemispheric hindcast runs with the Naval Research Laboratory Mountain Wave Forecast Model (MWFM) [Eckermann and Preusse, 1999]. This nonstandard MWFM product for the 1999/2000 Arctic winter has been used in previous CTM studies by Pierce *et al.* [2003] and Pagan *et al.* [2004], where full details of its synthesis are provided. Briefly, the nonhydrostatic ray-based version of the MWFM (also known as MWFM-2) was run each day in hindcast mode based on global  $1^\circ \times 1^\circ$  analyses issued by NASA's Global Modeling and Analysis Office. This multiray output is then averaged into  $1^\circ \times 1^\circ$  grid boxes to generate a mean peak temperature perturbation (MPTP) amplitude and standard

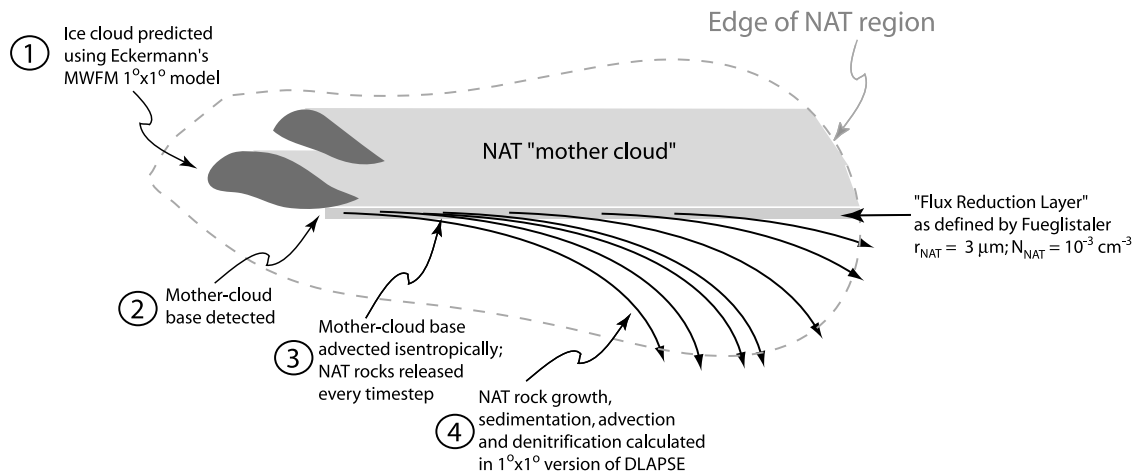


**Figure 1.** Schematic diagram of how the DLAPSE models nitric acid trihydrate (NAT) nucleation via mountain wave–induced mesoscale ice and the formation of mother clouds. MWFM is mountain wave forecast model. See color version of this figure in the HTML.

deviation that is more easily combined with analysis fields. For this study, we rederived the product to correct a small earlier error in this averaging procedure that affected grid boxes with only one ray within it: this produces very minor changes in synoptic MWFM MPTP maps. The daily (1200 UT) gridded MPTP output from the MWFM is issued on a  $1^\circ \times 1^\circ$  grid on pressure levels of 10, 20, 30, 40, 50, 70 and 100 hPa. Recently, Jiang *et al.* [2004] provided a detailed validation of global MWFM mesoscale temperature fluctuation hindcasts in the Arctic winter stratosphere by comparing them rigorously against mountain wave–related radiance perturbations derived from several years of stratospheric radiances acquired by the Microwave Limb Sounder (MLS) instrument on the Upper Atmospheric Research Satellite (UARS). As noted by Pagan *et al.* [2004], this grid box–averaged product tends to underestimate peak mountain wave variability, and as such probably represents a lower bound on actual stratospheric mountain wave temperature fluctuations.

### 2.3. Formation of Mountain Wave–Induced Mother Clouds

[13] The MWFM mean temperature fluctuation fields are combined with ECMWF analyzed synoptic temperatures to determine regions cold enough for mesoscale ice and hence form high number density NAT mother clouds on the downwind edge of the ice clouds. We then advect these mother clouds isentropically in a Lagrangian manner and numerically seed NAT particles at a lower number density at their base at each time step, which can then grow, sediment and cause denitrification (see section 2.4).

[14] The  $1^\circ \times 1^\circ$  SLIMCAT water vapor and pressure fields are used to give a 3-D field of  $T_{\text{ice}}$  using the expression from Hanson and Mauersberger [1988]. Grid boxes that are more than 3 K below the ice frost point after the mesoscale cooling has been added to the synoptic-scale temperature field are defined as containing an ice PSC [Carslaw *et al.*, 1998]. The ice PSC formation temperature has been investigated in a number of studies [e.g., Koop *et al.*, 2000] and we use the best estimate of  $T_{\text{ice}} - 3 \text{K}$  which has been used in several other modeling studies [e.g., Luo *et al.*, 2003]. As described in section 1, we assume that NAT

nucleates heterogeneously on these mesoscale ice clouds to form a high number density NAT “mother cloud” (see Figure 1). At each time step a new discrete mother cloud is created downwind of all mesoscale ice clouds. The geometric area of the mother cloud, which is required to calculate the rate of production of sedimenting particles (see below), is set equal to the area of a  $1^\circ \times 1^\circ$  grid box at  $60^\circ\text{N}$ . This assumed constant size of the mother cloud and the 1800 s time step corresponds to a zonal wind passing through the mountain wave at  $30.9 \text{m s}^{-1}$ , which is a reasonable speed for the conditions under which mesoscale ice clouds are formed [e.g., Carslaw *et al.*, 1998]. After formation, each mother cloud “element” is advected as an isentropic trajectory at the center of the cloud. Each mother cloud element then serves as the generation site for sedimenting NAT particles, as described in section 2.4.

### 2.4. NAT Sedimentation From Mother Clouds

[15] Fueglistaler *et al.* [2002a] introduced the concept of a “flux reduction layer” (FRL) at the base of the mother cloud where gas phase nitric acid depletion and particle acceleration through growth cause the number density to reduce to around  $10^{-3} \text{cm}^{-3}$  and average particle size to increase to  $3 \mu\text{m}$ . They used a high-vertical resolution 1-D numerical model to demonstrate that NAT particle number density and size in the FRL is relatively insensitive to the NAT particle number density in the mother cloud itself. We exploit this result to model NAT sedimentation from mother clouds at much lower vertical resolution than was used by Fueglistaler *et al.* [2002a]. Sedimenting NAT particles are introduced into the model at the altitude of the FRL (base of the mother cloud) at a radius of  $3 \mu\text{m}$  and with a concentration of  $10^{-3} \text{cm}^{-3}$  [Fueglistaler *et al.*, 2002a]. As these particles grow and sediment the change in gas phase  $\text{HNO}_3$  is calculated on the  $1^\circ \times 1^\circ$  SLIMCAT grid. The variation of particle size and gas phase  $\text{HNO}_3$  with altitude is much slower below the FRL than in it. By beginning our simulation at the base of the FRL and imposing particle properties from Fueglistaler *et al.* [2002a] we avoid the need for a very high resolution model.

[16] Several hundred thousand sedimenting NAT particles are typically simulated in DLAPSE, with each particle

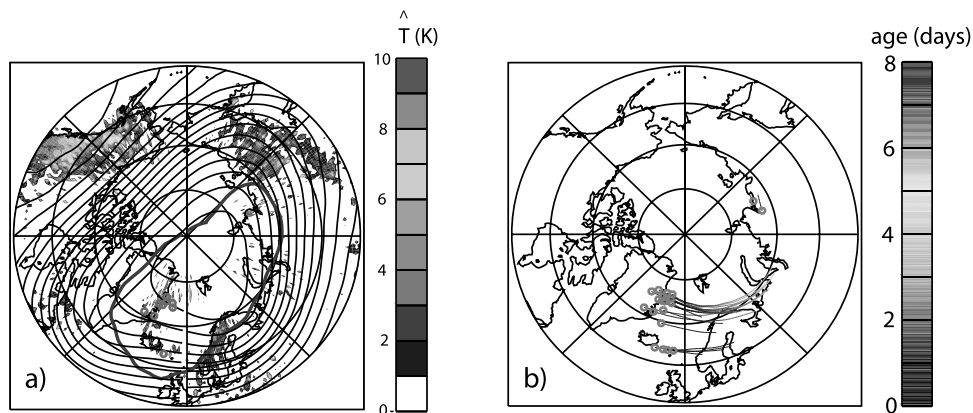


**Figure 2.** (a) Map of gridded MWM temperature perturbation for 20 December 1999 on the 30 hPa pressure surface. Also marked are the contour of  $T = T_{\text{NAT}}$  (red line) and flow streamlines (black lines). Note that streamlines are lines of constant geopotential on this constant pressure surface from European Centre for Medium-Range Weather Forecasts (ECMWF) analyses. Also shown as pink open circles in Figure 2a are the nucleation points for mother cloud bases between 30 and 40 hPa when this mountain wave cooling is added to the temperature from the ECMWF analyses as described in section 2.3. (b) Trajectories of mother cloud bases at all altitudes which formed on 20 December 1999 at 1200 UT. See color version of this figure in the HTML.

standing for a very large number of real particles. In our previous simulations, in which NAT was produced evenly through the NAT region, the scaling factor (real particles per model particle) was deduced by iteratively running the model with a different scaling factor (i.e., nucleation rate) until best agreement was reached with particle observations on 20 January 2000 [Carslaw *et al.*, 2002]. In these mother cloud simulations the scaling factor can be determined physically from the downward NAT flux in the FRL and the size of the mother cloud. With each mother cloud covering an area  $A_{60N}$  equivalent to one SLIMCAT grid box at  $60^\circ\text{N}$ , the scaling factor is  $Nv_zA_{60N}\Delta t$ , where  $N$  is the number concentration at the base of the FRL ( $10^{-3}\text{ cm}^{-3}$ ) and  $v_z$  is the sedimentation speed of the  $3\text{ }\mu\text{m}$  particles ( $0.0051\text{ m s}^{-1}$ ). This scaling factor means that in one time step,  $Nv_zA_{60N}\Delta t$  real particles will fall from the FRL into the grid box below and in the model these sedimenting particles are represented by one particle produced at that altitude. The 3-D advection and sedimentation of the model particle is subsequently tracked and more such particles are produced at the FRL altitude until the mother cloud evaporates (exits the NAT supersaturated region).

[17] Because grid boxes get smaller toward the pole, the amount of  $\text{HNO}_3$  removed from the gas phase of each grid box by particle growth will be much larger there than at  $60^\circ\text{N}$ . To guard against this effect the change in  $\text{HNO}_3$  caused by the growth of the model particles is distributed equally among a number of neighboring grid boxes whose total area matches  $A_{60N}$ . Effectively, this means that the mother cloud area (and the concentration of sedimenting particles seeded below the cloud) is conserved during advection, as it physically should be.

[18] It remains to explain how the mother cloud base is located. We assume the wind is zonal and consider each longitude-altitude slice separately. Figure 1 shows a schematic of one such slice with the ice PSC region shaded in darker blue. In the situation shown, there are two vertically overlapping ice regions which would each produce stream-

ers of NAT downstream (shown as the lighter blue region in Figure 1). In such a case, the two downstream mother clouds would together form one continuous high number density “mother cloud region” with only one mother cloud base. An algorithm was developed to find the downstream lower corner of all such mother cloud regions. This corner is defined as the mother cloud base, which is then advected.

[19] For the comparison run, we model denitrification using a constant volume average NAT nucleation rate of  $8.1 \times 10^{-10}\text{ particles cm}^{-3}\text{ s}^{-1}$ , which has been shown to reproduce very well changes in the particle number concentration observed in the period January to March 2000 [Carslaw *et al.*, 2002] and produce denitrification that matches a wide range of measurements for previous winters [Davies *et al.*, 2005]. For this comparison run, NAT particles are initialized with a radius of  $0.1\text{ }\mu\text{m}$ .

### 3. Results

#### 3.1. Mountain Waves and NAT Mother Cloud Formation

[20] Figure 2a shows the gridded mountain wave perturbation field on the 30 hPa pressure level for 20 December 1999 1200 UT as prescribed by MWM. Also marked are lines of constant geopotential indicating the streamlines of the flow (in black) and the contour for the NAT equilibrium temperature (in red) from the ECMWF analyses, the latter calculated using the SLIMCAT gas phase nitric acid and water vapor concentrations following Hanson and Mauersberger [1988]. At this time, mountain waves can be seen over Alaska, western United States and Canada, Greenland, Iceland, the Norwegian mountains and Siberia. The gridded temperature perturbation caused by the mountain waves can be as large as 10 K (although at this time the maximum temperature perturbation on this day is around 5 K).

[21] At this time, the area of possible NAT formation ( $T < T_{\text{NAT}}$ ) is large, centered around Spitzbergen, covering most of Greenland and stretching over northern Scandinavia reaching

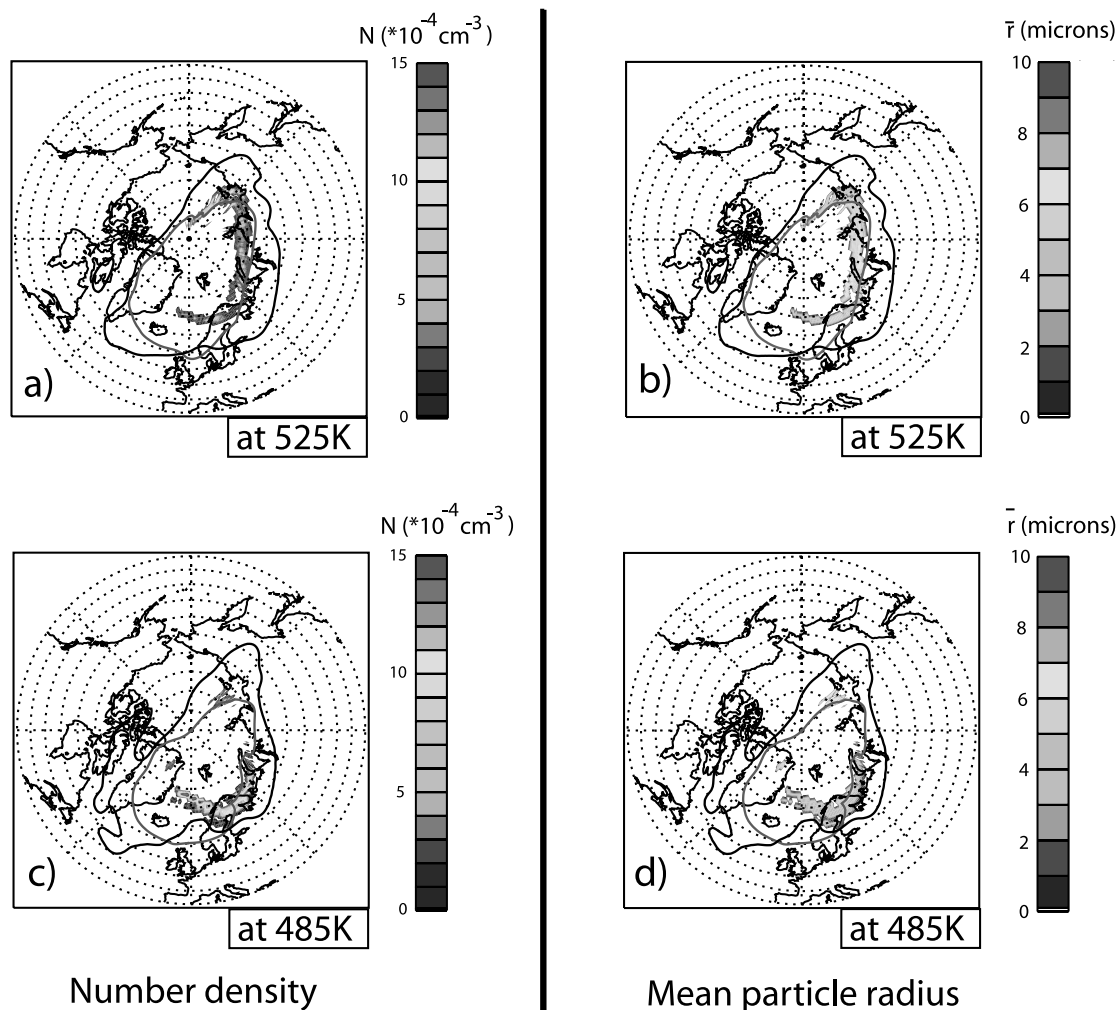


**Figure 3.** Maps of model NAT particle number density and mean radius for the 525 K and 485 K potential temperature layers as on 21 December 1999 at 1200 UT. Also marked are the line indicating the NAT equilibrium temperature, calculated using the expression of *Hanson and Mauersberger* [1988] (in red) and the vortex edge taken to be at  $65^\circ$  equivalent latitude (black). See color version of this figure in the HTML.

Siberia. The pink circles in Figure 2a indicate the horizontal position of the mother cloud bases found between 30 and 40 hPa using the algorithm described in section 2.4. The streamlines indicate the initial direction in which each mother cloud (base) will be advected after it has formed.

[22] Figure 2b shows the trajectories of the mother cloud bases that formed at 1200 UT on 20 December 1999 over all pressures. The pink circles indicate the initial (nucleation) position of the mother clouds, i.e., the position of the ice cloud corners (see section 2.4). Mother clouds are formed on the eastern coast of Greenland and Iceland, where there is significant mountain wave activity colocated with air strongly supersaturated with respect to NAT. In addition, two mother clouds have formed over Arctic Russia. As indicated by the streamlines in Figure 2a, mother clouds formed over Greenland and Iceland are advected east toward Scandinavia and last from 2 to 4 days before the air temperature rises above the  $T_{\text{NAT}}$ . Those formed over Siberia also head east but stay below  $T_{\text{NAT}}$  for only a few hours. At each time step on these trajectories, each mother cloud base will release a sediment-

ing “model” NAT particle of  $3 \mu\text{m}$  radius with a scaling factor, which corresponds to a number density of  $0.001 \text{ cm}^{-3}$  over an area  $A_{60N}$  (see section 2.4). This model particle then grows or evaporates depending on saturation conditions, and is advected and sedimented accordingly. As the particle grows/shrinks, it removes/adds an amount of nitric acid from/to the gas phase given by its scaling factor. Mother clouds are assumed to evaporate as soon as they enter air, which is subsaturated with respect to NAT, at which point their trajectories are curtailed and the sedimenting NAT particles cease to be released.

### 3.2. Spatial Coverage, Concentrations, and Size of Sedimenting NAT Particles

[23] Figure 3 shows a snapshot of NAT number density and mean radius at two altitudes on 21 December 1999. This date is near the start of the long cold period in this Arctic winter, but already a large NAT supersaturated region (marked by the red line) is apparent. Consequently, NAT particles that sediment from mother clouds inside

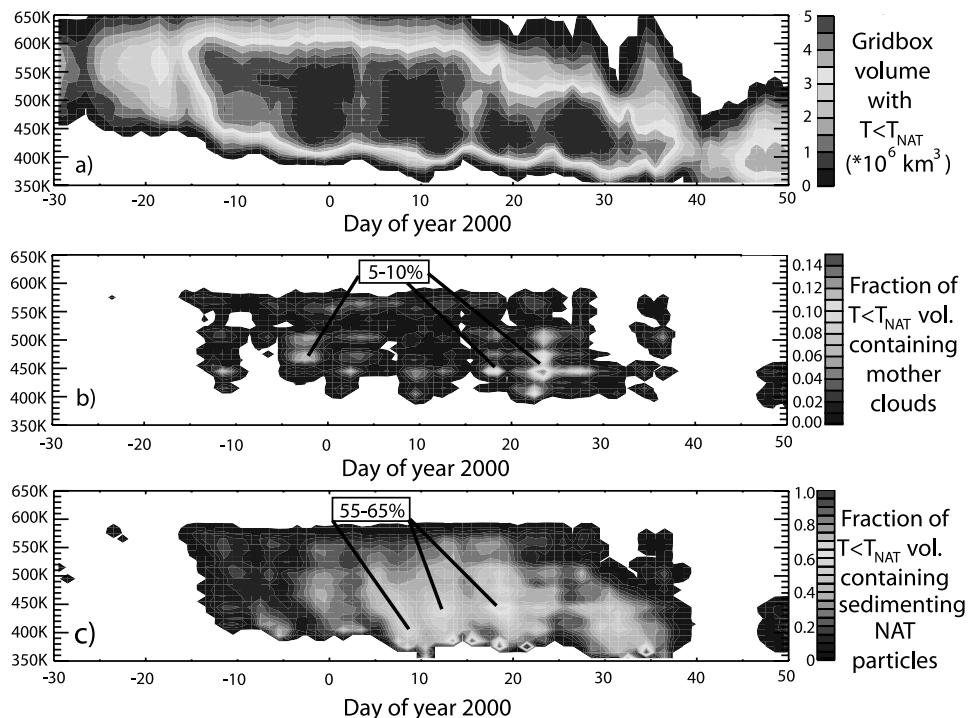


**Figure 4.** Time-altitude plots of (a) grid box volume supersaturated with respect to NAT and the fraction of this volume containing (b) high number density NAT mother clouds and (c) low number density NAT rocks. In each plot, values that are less than 0.001 are indicated as white. See color version of this figure in the HTML.

this region will start to grow larger than their initial radius of  $3 \mu\text{m}$  and commence denitrification. The contour of the polar vortex edge (indicated by the black line) is concentric with the NAT region at this time and continues to be so for several days. As demonstrated by Mann *et al.* [2002, 2003], this concentricity indicates that there is a large region of cold closed flow, hence the sedimenting NAT particle trajectories will tend to remain in the growth region for several days and there will be efficient denitrification if there are sufficient mother clouds to act as a source of sedimenting NAT.

[24] At the 485 K level, a streamer of sedimenting NAT particles can be seen coming off Greenland, trailing over Norway, Sweden, Finland and into Russia. These particles are those that have sedimented from the base of mother clouds like those in Figure 2 which were originally caused by mountain waves over Greenland. The particles have number density at around  $0.001 \text{ cm}^{-3}$  and mean radius of between 3 and  $5 \mu\text{m}$ . The larger NAT particles will be older and will have fallen from mother clouds at a higher altitude. At this time, these large NAT particles produced via the mother cloud mechanism have only a low coverage of the NAT region.

[25] At the 525 K level, a similar streamer exists that extends farther east. These particles have been sedimented from a different mother cloud (at a different altitude) than those at the 485 K level. On average, the particles are larger than those at the 485 K level and the larger particles will have been formed at a higher altitude. Note also that the number density has reduced to  $2\text{--}4 \times 10^{-4} \text{ cm}^{-3}$ . In this way, the mother cloud mechanism can produce large

variations in particle concentration and size because of the heterogeneity of the mother cloud distribution and the different ages of the sedimenting particles. By contrast, for DLAPSE simulations using the constant volume average nucleation mechanism, the mean radius increases with decreasing height throughout the NAT region creating a more homogeneous particle field (not shown).

[26] Figure 4 gives a more complete picture of the evolution and coverage at all levels over the entire winter. Shown are the total grid box volume below the NAT equilibrium temperature, the fraction of this volume that contains mother clouds, and the fraction of this volume that contains sedimenting NAT.

[27] In this simulation, the maximum coverage of mountain wave-induced mother clouds reaches only  $\sim 5\text{--}10\%$  of the NAT region. This small fraction is broadly in agreement with the results of the 1994/1995 Arctic winter given by Carslaw *et al.* [1999]. In contrast, at the times with the widest coverage in the middle of January, around  $55\text{--}65\%$  of the NAT region contains sedimenting NAT particles that have fallen from the mother clouds. This peak coverage occurs at a time when the NAT region has been large, deep and concentric with the polar vortex for several weeks [see Mann *et al.*, 2003]. The coverage of sedimenting NAT is larger than the NAT mother clouds because the sedimenting NAT fills the volume below the mother clouds, whereas the NAT in the mother clouds is advected isentropically. Notice that the times of peak coverage of NAT clouds do not coincide with the peak coverage of mother clouds. Mother cloud coverage increases with time only when mountain wave ice clouds exist, while each mother cloud, once produced, creates an ever increasing coverage of

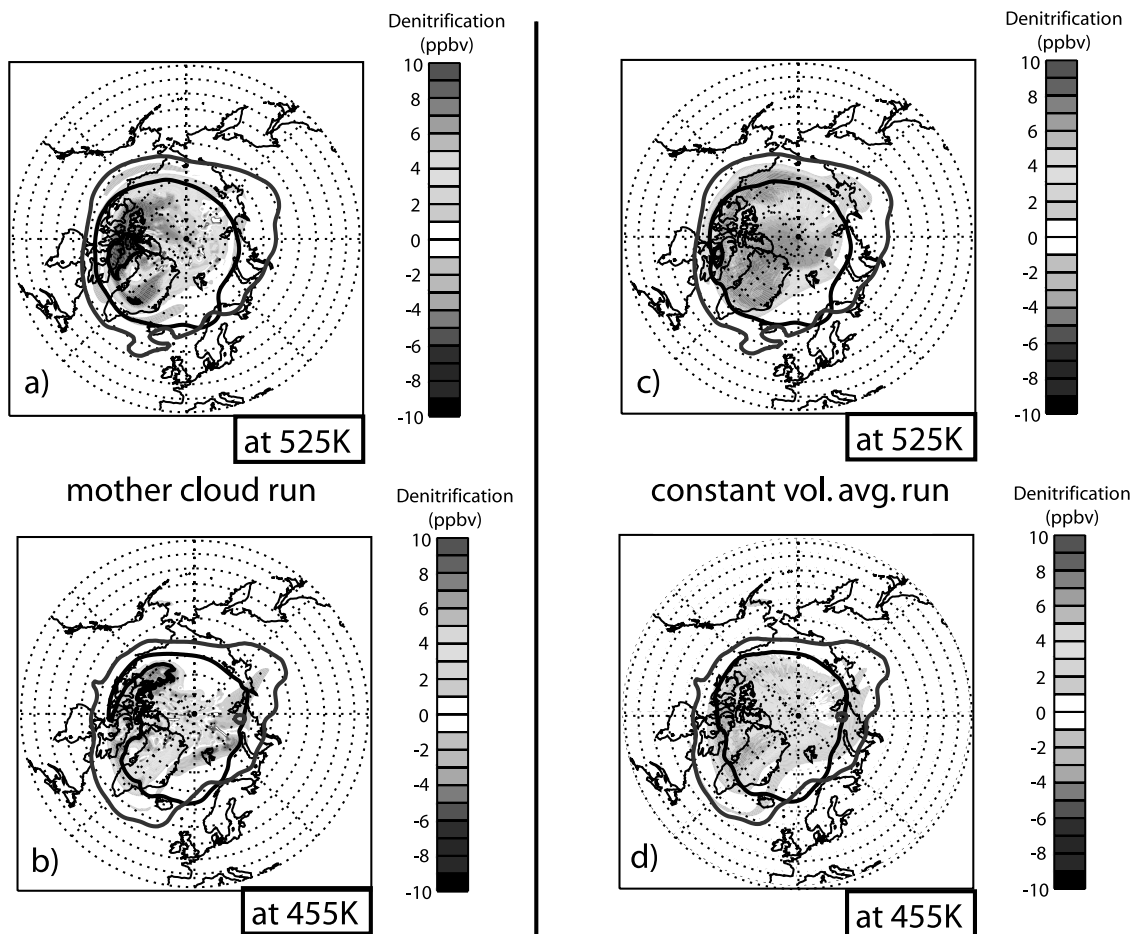


**Figure 5.** Contour plots of denitrification at 1200 UT on 10 January 2000 for the mountain wave-induced mother cloud run at (a) 525 K and (b) 455 K and for the constant volume average nucleation run at (c) 525 K and (d) 455 K. The contour of  $T = T_{\text{NAT}}$  is marked as a black contour, and the vortex edge ( $65^\circ$  equivalent latitude) is marked as a blue contour. See color version of this figure in the HTML.

sedimenting particles below it. In addition, mother clouds evaporate as soon as  $T > T_{\text{NAT}}$ , whereas the large NAT particles can take significant time to evaporate in NAT subsaturated air, during which time they may be advected back into supersaturated air and begin growing again. Examination of the day-by-day particle fields shows that this occurs on many occasions.

[28] Pagan *et al.* [2004] showed that large-scale NAT PSCs observed by the DC-8 on 5, 7, and 10 December 1999 could not have been caused by mountain waves. These dates (at 1200 UT) correspond to days  $-26.5$ ,  $-24.5$  and  $-21.5$  in Figure 4. The results of our simulation support this conclusion, since the volume with  $T < T_{\text{NAT}}$  is completely free from mountain wave-induced NAT at these times (white contour means the volume fraction containing NAT is less than 0.001 in Figure 4c).

### 3.3. Denitrification Caused by Mountain Waves

[29] We now investigate how much denitrification these mountain wave-induced sedimenting NAT particles can cause and compare this with a simulation where large NAT particles are produced using the simple constant volume average nucleation mechanism. The DLAPSE denitrification simulation for this winter using a constant

volume average NAT nucleation rate is described in detail by Mann *et al.* [2003]. Briefly, a large, deep NAT region concentric with the polar vortex begins in late December, persisting through much of January, enabling prolonged NAT growth and sedimentation for up to 3 weeks once nucleation has occurred.

#### 3.3.1. Distribution of Denitrification

[30] We now compare denitrification due to the two nucleation mechanisms at two different times in the winter. The first date is 10 January 2000, which is in the middle of the 3-week period of intense denitrification. The second is 20 January 2000, which is at the end of this 3-week period, by which time the denitrification is very strong and gas phase nitric acid amounts are very low over large areas of the vortex. In times of such low concentrations of nitric acid, the denitrification becomes limited by the supply of nitric acid [see Mann *et al.*, 2003].

[31] Note that in Figures 5–8, denitrification is calculated as the passive nitric acid concentration minus the nitric acid concentration summed over the gas phase, solid NAT phase and liquid STS phase. (Negative values indicate reinitiation.)

[32] Figure 5 shows maps of denitrification on the 525 K and 455 K isentropic surfaces for each of the two DLAPSE

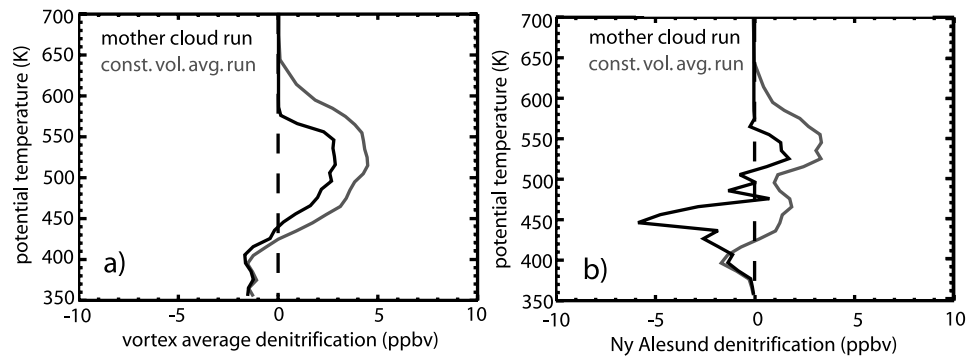


**Figure 6.** Profiles of denitrification at 1200 UT on 10 January 2000 for the mountain wave-induced mother cloud run (black line) and the constant volume average run (red line) as a (a) vortex average and (b) point profile at Ny Alesund ( $78.9^{\circ}\text{N}$ ,  $12.0^{\circ}\text{E}$ ). See color version of this figure in the HTML.

model runs on 10 January 2000 at 1200 UT. At this time, at both levels, there is a very large area below the NAT equilibrium temperature (shown by the black solid line), which is also very concentric with the polar vortex producing a large, deep region of cold closed flow. The simulation where NAT is sedimented from locally produced mother clouds has

much more heterogeneous denitrification field than the simulation where NAT is produced slowly throughout the vortex. The maximum denitrification (red) at this time is stronger in the mother cloud run although it is more widespread in the constant volume average run. In the mother cloud run there are also regions of renitrification (blue) even at the 525 K

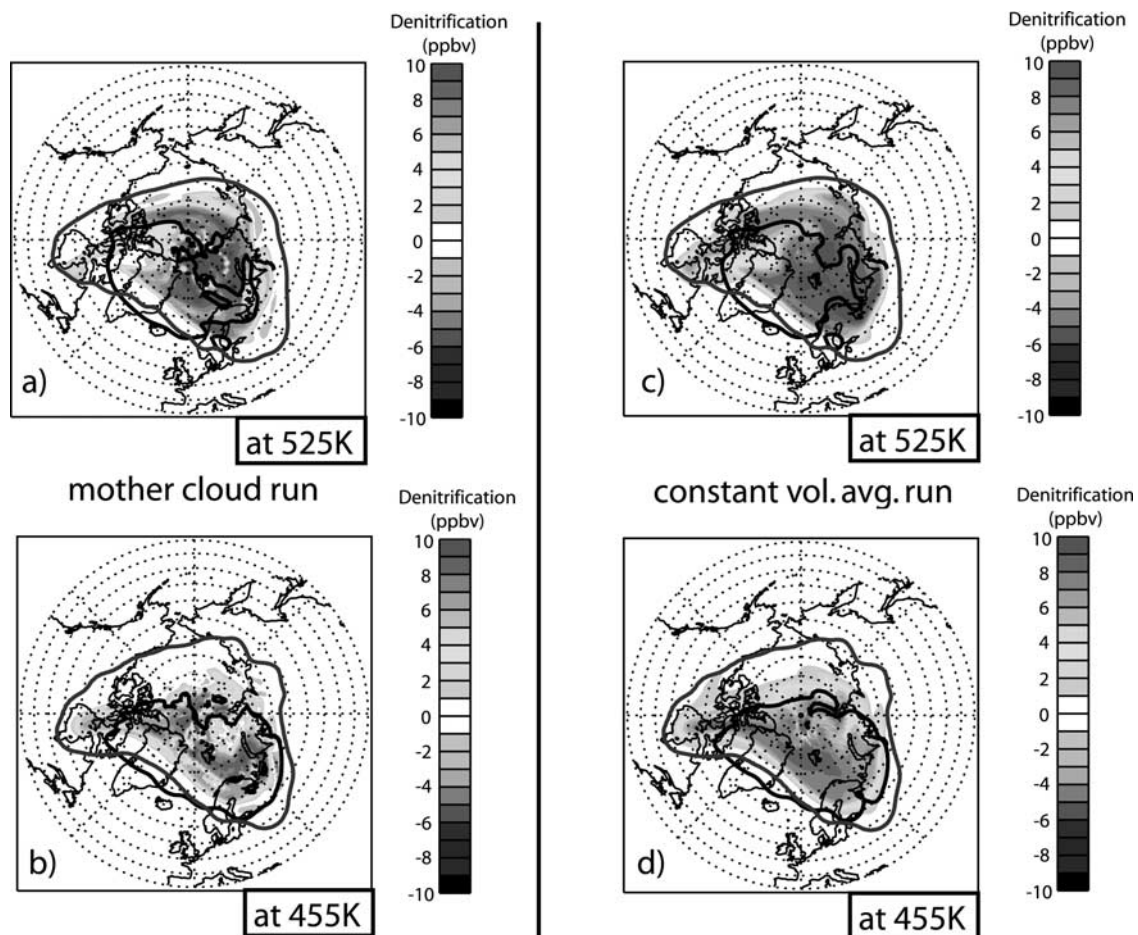


**Figure 7.** Contour plots of denitrification at 1200 UT on 20 January 2000 for the mountain wave-induced mother cloud run at (a) 525 K and (b) 455 K and for the constant volume average nucleation run at (c) 525 K and (d) 455 K. The contour of  $T = T_{\text{NAT}}$  is marked as a black contour, and the vortex edge ( $65^{\circ}$  equivalent latitude) is marked as a blue contour. See color version of this figure in the HTML.

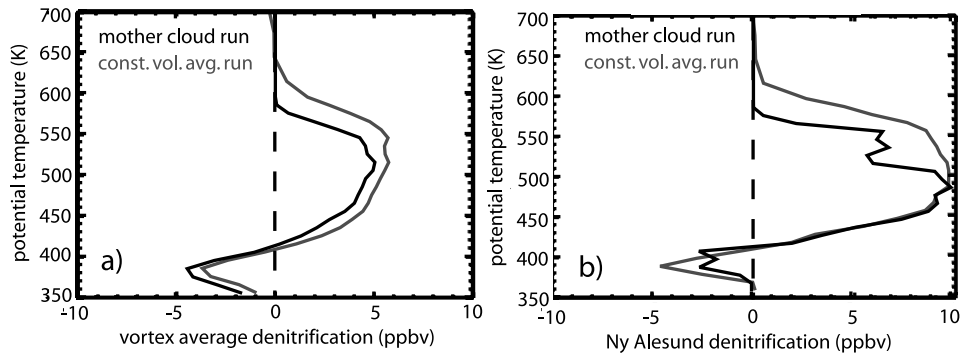


**Figure 8.** Profiles of denitrification at 1200 UT on 20 January 2000 for the mountain wave-induced mother cloud run (black line) and the constant volume average run (red line) as a (a) vortex average and (b) point profile at Ny Alesund ( $78.9^{\circ}\text{N}$ ,  $12.0^{\circ}\text{E}$ ). See color version of this figure in the HTML.

level, whereas renitrification only occurs in the levels below around 430 K in the constant volume average run.

[33] Figure 6 shows profiles of denitrification for the two runs as an average over the entire vortex (Figure 6a) and interpolated to Ny Alesund ( $78.9^{\circ}\text{N}$ ,  $12.0^{\circ}\text{E}$ ) (Figure 6b). Comparing the vortex average denitrification profiles, the mother cloud run typically has shallower, less strong (around 50% lower at peak) denitrification than the constant vortex average run at this time. However, as seen in Figure 5, there are areas where the denitrification is higher in the mother cloud run. At this time, in the mother cloud simulation, there is a streak of renitrified air over Ny Alesund at 455 K (see Figure 5b). The depth of this streamer can be seen in Figure 6b to be around 30 K and is up to 6 ppbv renitrified compared to the passive nitric acid tracer at the 445 K level.

[34] Figure 7 shows maps of denitrification on two isentropic surfaces for each of the two DLAPSE model runs for 20 January 2000 at 1200 UT. Although the sedimenting NAT particles in the mother cloud run are produced from thin streamers of mother clouds, the NAT mother clouds and sedimenting particles have such long lifetimes that many of them have now circulated around the vortex more than once. In such conditions, the mother clouds can exist at many levels and the sedimented NAT particles can cover up to 60% of the vortex (see Figure 4c) and hence the polar vortex becomes very strongly denitrified throughout this region of recirculation. Notice also that the contour indicating the edge of the NAT region has been contorted because the gas phase nitric acid has been depleted to near zero in the denitrified part of the vortex. Consequently, at this time, the fields of denitrification for the two runs are remarkably similar despite the very different production mechanisms.

[35] Figure 8a shows profiles of the vortex average denitrification which has occurred by 1200 UT on 20 January 2000 for each of these runs. The profiles of denitrification for the two cases are also very similar for the two simulations, with the vortex having now been very strongly denitrified in each case, although the denitrification in the mother cloud run is slightly weaker (about 20% lower at peak) and shallower. The denitrification profiles at Ny Alesund are almost identical below 500 K (see Figure 8b) since it is in the very strongly denitrified core of the vortex at this time.

[36] Considering a column integration of the denitrified part of the vortex average profile, we can say that the mother cloud run has about 70% of the total denitrification of the constant volume average run. *Davies et al.* [2005] have shown that the DLAPSE model, when run with this constant volume average nucleation rate matches the denitrification observed by the  $\text{NO}_y$  instrument aboard the high-altitude ER-2 aircraft on the several flights that took place between 20 January and 11 March 2000. Although a detailed comparison with observations is outside the scope of this study, these simulations suggest that the mother cloud mechanism may be able to account for as much as 80% of the observed denitrification for this winter. It should be noted, however, that the ER-2 flights only sampled air in the lowest part of the stratosphere (below around 475 K) and all flights took place after the denitrification was almost complete.

### 3.3.2. Winter-Long Evolution of Denitrification

[37] Figures 9 and 10 show how the vortex average NAT particle number density, mean radius and denitrification vary with height and time throughout the winter. The number density and mean particle radii calculations are averages of grid box mean values over the NAT region and do not include the contribution of NAT particles contained within the mother clouds themselves (which have concentrations as high as  $10\text{ cm}^{-3}$ ). Instead, they only represent the average values for particles which have sedimented out of the base of the flux reduction layer below the mother cloud. We refer to these as “sedimenting NAT particles” to distinguish them from those in the mother cloud itself. Figures 9 and 10 convey the general evolution of the extent of denitrification in the vortex alongside changes in the sedimenting NAT field for each of the two NAT production mechanisms.

[38] For the model run using the mountain wave-induced mother cloud mechanism, significant numbers of sedimenting NAT particles do not appear until around day -15 (16 December 1999) when widespread mother clouds first occur. When the constant volume average nucleation mechanism is used, sedimenting NAT is present at some point in the vortex right from the start of the run. This is because temperatures were low enough throughout December 1999 that the Arctic vortex always had a nonzero volume supersaturated with respect to NAT (see Figure 4). Consequently, denitrification begins in the mother cloud nucleation run about 2 weeks later than in the large-scale nucleation run.

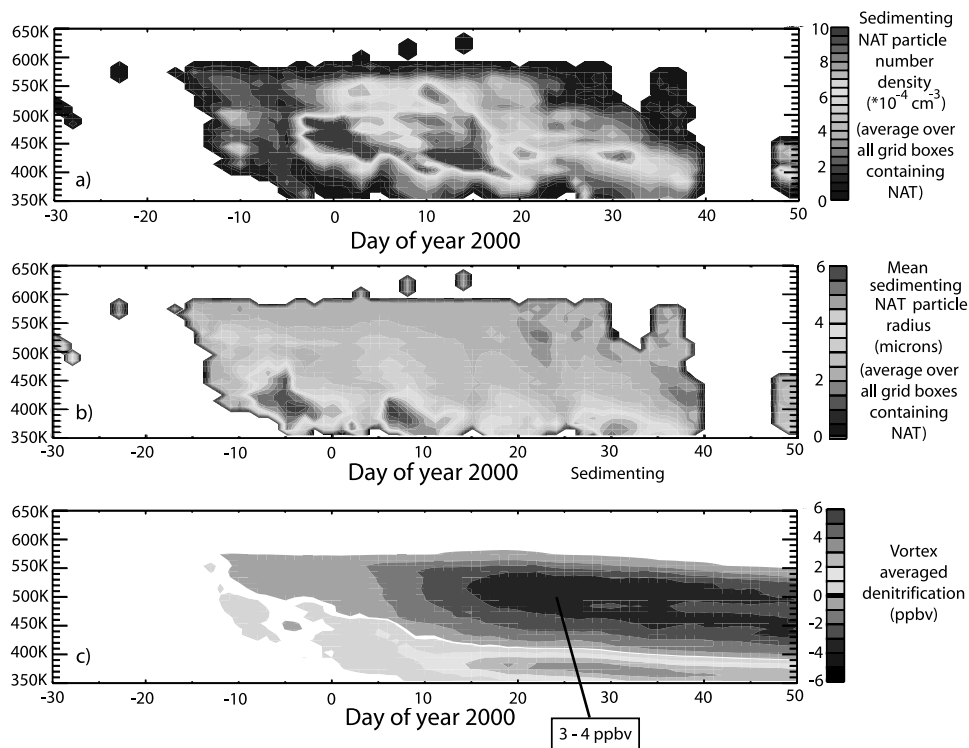


**Figure 9.** Time-altitude curtain plots of sedimenting NAT particle number density, mean radius, and denitrification for the mountain wave-induced mother cloud run. Note that the denitrification is an average over the vortex, but the mean particle radii and number density are over grid boxes which contain NAT particles. See color version of this figure in the HTML.

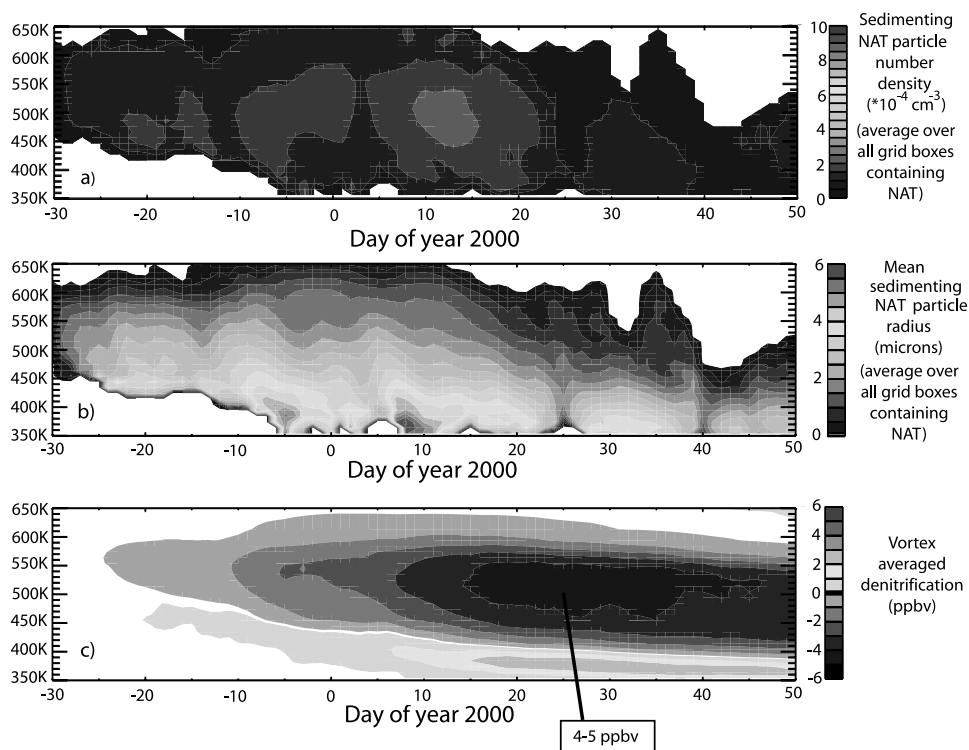


**Figure 10.** Time-altitude curtain plots of sedimenting NAT particle number density, mean radius, and denitrification for the large-scale nucleation run. Note that the denitrification is an average over the vortex, but the mean particle radii and number density are over grid boxes which contain NAT particles. See color version of this figure in the HTML.

[39] In the mother cloud run, the pattern of sedimenting NAT concentration initially matches the pattern of sedimenting NAT production (see Figure 4c). However, as the mother clouds become well distributed around the vortex (because of the prolonged cold closed flow situation) the average number density of sedimenting NAT increases significantly occasionally reaching concentrations as high as  $10^{-3} \text{ cm}^{-3}$ . These number density peaks are in the vertical range 450–500 K on 28 December to 4 January 2000 and 400–500 K on 10–17 January 2000. When the number concentration becomes this high (because of accumulation of particles), almost all of the nitric acid can be in the solid NAT phase. Consequently, the ability for NAT particles recently sedimented from the mother cloud base to grow larger is restricted, and the mean NAT rock radius actually reduces despite this ongoing cold concentric closed-flow situation. This anticorrelation can be seen in Figures 9a and 9b. The number densities span the observed number density range reported by *Northway et al.* [2002] of between  $10^{-5}$  and  $10^{-3} \text{ cm}^{-3}$ .

[40] The maximum vortex average denitrification over this time period reaches 3–4 ppbv for the mother cloud run compared with 4–5 ppbv for the constant volume average run. The simulations suggest that denitrification by NAT particles sedimented from mountain wave-induced mother clouds may be responsible for a considerable proportion of the observed denitrification. In addition, large NAT particles produced in this way may help to explain the variability in aircraft observations of denitrification that are not captured by the large-scale nucleation mechanism used by *Davies et al.* [2005].

#### 4. Limitations of This Study

[41] This study suggests that the low number density NAT particles produced by mountain wave-induced mother clouds have the potential to cause widespread denitrification and are sufficient to explain the bulk of the magnitude of observed denitrification in 1999/2000.

[42] The following caveats should be borne in mind when considering these results. Our mother cloud simulation here is somewhat simplified since no attempt is made to account for overlapping mother cloud streamers, which are likely to occur in prolonged cold closed flow situations. In such cases, NAT particles would not continue to sediment from both of the overlapping cloud bases and we will overestimate large particle production and subsequent denitrification. Second, the magnitude of denitrification is determined by the size of the mother clouds, which is, in turn, determined by the size of the mountain wave-induced ice clouds which generate them. We have assumed the ice clouds to have an along-ridge size of  $\sim 110 \text{ km}$ , which was determined by the highest horizontal resolution of our model of  $1^\circ \times 1^\circ$ . This size of cloud is sufficient to capture the major wave events over Scandinavia and eastern Greenland, but it will overestimate the influence of much smaller isolated wave clouds. Because of the feedback between particle growth and gas phase  $\text{HNO}_3$ , which is carried on the  $1^\circ \times 1^\circ$  CTM grid, it is not straightforward to capture denitrification occurring as a subgrid process. Third, we have not accounted for the complete loss of particles from the mother clouds. These issues mean that the model could

overestimate denitrification caused by mountain waves. However, other factors that we have not accounted for could lead to an underestimate. For example, we make no attempt to include the effects of wind shear on the evolution of the mother clouds. Vertical wind shear will tend to increase their vortex areal coverage, although increasing the area will also decrease the length of time over which the mother clouds can supply sedimenting particles to the air below. In addition, the gridding of the temperature perturbations leads to a reduction in peak amplitude, which may partly compensate for overestimating the area of the waves.

#### 5. Conclusions

[43] We have developed a method of simulating the production of large, low number density NAT particles via the nucleation of mountain wave-induced NAT mother clouds within the 3-D microphysical, Lagrangian denitrification model DLAPSE. The nonhydrostatic mountain wave forecast model MWFM [*Eckermann and Preusse, 1999*] is used to provide the mesoscale cooling field. Streamers of NAT mother clouds form from mesoscale patches of ice, which then sediment out moderate sized NAT particles at low number concentration. The denitrification caused by subsequent growth, advection and sedimentation of these particles is calculated by the DLAPSE model, which is coupled to the 3-D off-line chemical transport model SLIMCAT. Denitrification caused by low number density NAT particles produced by this mechanism is modelled at high ( $1^\circ \times 1^\circ$ ) resolution on the vortex scale for the 1999/2000 winter.

[44] Although the high number density NAT mother clouds themselves only cover a maximum of 5–10% of the NAT supersaturated region at any one level, sedimentation of NAT particles from the base of these mother clouds enhances the maximum coverage to over 60%. Consequently, even though the large NAT particles are produced by small-scale temperature perturbations due to mountain waves, they can become widespread across the NAT supersaturated region if the meteorology is optimum (concentric regions of low temperature and wind flow, leading to long particle lifetimes). These estimated coverages are close to those derived from airborne lidar observations [*Toon et al., 2000*]. Future work should examine whether the microphysical properties of the model clouds are similar to those observed. However, our results do not contradict the findings of *Pagan et al.* [2004] that large-scale NAT PSCs observed by airborne lidar in early December 1999 could not have been caused by mountain waves.

[45] Denitrification caused by sedimenting NAT particles produced in this way has been compared with that caused by NAT generated by a simple volume average nucleation mechanism, which has been shown to broadly reproduce the extent and timing of denitrification observed for several recent cold Arctic winters [*Davies et al., 2005*]. As such, this control model run is used as a proxy for the actual denitrification, which has taken place at that time.

[46] Using this approach, this modeling study has suggested that as much as 80% of the denitrification observed in the 1999/2000 winter could have been caused by NAT particles sedimented from high number density mother clouds nucleated on mesoscale ice clouds pro-

duced by mountain wave temperature fluctuations. Comparison between the timing of denitrification for the two nucleation mechanisms suggests that mountain wave-induced denitrification occurs around 2 weeks later than if a constant volume average NAT nucleation mechanism is invoked.

[47] Large NAT particles produced by small-scale mountain wave processes result in greater inhomogeneities in the denitrification field, which may help to explain some of the large variability seen in observations that has not been captured by a large-scale nucleation mechanism [Davies *et al.*, 2005]. An examination of scales of variability of particles and HNO<sub>3</sub> might shed some light on the solid particle production mechanism. It is worth stressing that whichever nucleation mechanism is used, the dominant factor controlling the extent of denitrification is clearly the meteorology and in particular the existence of a region of cold closed flow [Mann *et al.*, 2003] in which particles can recirculate and grow in the vortex for extended periods.

[48] **Acknowledgments.** This work was funded by the European Commission Fifth Framework Program MAPSCORE (EVK2-CT-2000-00072) and EUPLEX (EVK2-2001-00119) projects and by the UK Natural Environment Research Council. We would also like to acknowledge useful discussions with Niels Larsen regarding this work.

## References

- Biele, J., A. Tsias, B. P. Luo, K. S. Carslaw, R. Neuber, G. Beyerle, and T. Peter (2001), Nonequilibrium coexistence of solid and liquid particles in Arctic stratospheric clouds, *J. Geophys. Res.*, *106*(D19), 22,991–23,007.
- Carslaw, K. S., B. P. Luo, and T. Peter (1995), An analytic expression for the composition of aqueous HNO<sub>3</sub>–H<sub>2</sub>SO<sub>4</sub> stratospheric aerosols including gas-phase removal of HNO<sub>3</sub>, *Geophys. Res. Lett.*, *22*, 1877–1880.
- Carslaw, K. S., M. Wirth, A. Tsias, B. P. Luo, A. Dornbrack, M. Leutbecher, H. Volkert, W. Renger, J. T. Bacmeister, and T. Peter (1998), Particle microphysics and chemistry in remotely observed mountain polar stratospheric clouds, *J. Geophys. Res.*, *103*(D5), 5785–5796.
- Carslaw, K. S., T. Peter, J. T. Bacmeister, and S. D. Eckermann (1999), Widespread solid particle formation by mountain waves in the Arctic stratosphere, *J. Geophys. Res.*, *104*(D1), 1827–1836.
- Carslaw, K. S., J. Kettleborough, M. J. Northway, S. Davies, R.-S. Gao, D. W. Fahey, D. G. Baumgardner, M. P. Chipperfield, and A. Kleinböhl (2002), A vortex-scale simulation of the growth and sedimentation of large nitric acid particles observed during SOLVE/THESEO 2000, *J. Geophys. Res.*, *107*(D20), 8300, doi:10.1029/2001JD000467.
- Chipperfield, M. P. (1999), Multiannual simulations with a three-dimensional chemical transport model, *J. Geophys. Res.*, *104*(D1), 1781–1805.
- Davies, S. (2003), Denitrification and ozone loss, Ph.D. thesis, Univ. of Leeds, Leeds, U. K.
- Davies, S., G. W. Mann, K. S. Carslaw, M. P. Chipperfield, J. A. Kettleborough, M. L. Santee, H. Oelhaf, G. Wetzel, Y. Sasano, and T. Sugita (2005), 3-D microphysical model studies of Arctic denitrification: Comparison with observations, *Atmos. Chem. Phys.*, *5*, 347–393.
- Dhaniyala, S., K. A. McKinney, and P. O. Wennberg (2002), Lee-wave clouds and denitrification of the polar stratosphere, *Geophys. Res. Lett.*, *29*(9), 1322, doi:10.1029/2001GL013900.
- Drdla, K., M. R. Schoeberl, and E. V. Browell (2002), Microphysical modelling of the 1999–2000 Arctic winter: 1. Polar stratospheric clouds, denitrification, and dehydration, *J. Geophys. Res.*, *107*, 8312, doi:10.1029/2001JD000782 [printed 108 (D5), 2003].
- Eckermann, S. D., and P. Preusse (1999), Global measurements of stratospheric mountain waves from space, *Science*, *286*, 1534–1537.
- Fahey, D. W., *et al.* (2001), The detection of large HNO<sub>3</sub>-containing particles in the winter arctic stratosphere and their role in denitrification, *Science*, *291*, 1026–1031.
- Fueglistaler, S., B. P. Luo, C. Voigt, K. S. Carslaw, and T. Peter (2002a), NAT-rock formation by mother clouds: A microphysical model study, *Atmos. Chem. Phys.*, *2*, 93–98.
- Fueglistaler, S., *et al.* (2002b), Large NAT particle formation by mother clouds: Analysis of SOLVE/THESEO-2000 observations, *Geophys. Res. Lett.*, *29*(12), 1610, doi:10.1029/2001GL014548.
- Hanson, D., and K. Mauersberger (1988), Laboratory studies of the nitric acid trihydrate: Implications for the south polar stratosphere, *Geophys. Res. Lett.*, *15*(8), 855–858.
- Hu, R. M., K. S. Carslaw, C. Hostetler, L. R. Poole, B. P. Luo, T. Peter, S. Fueglistaler, T. J. McGee, and J. F. Burris (2002), Microphysical properties of wave polar stratospheric clouds retrieved from lidar measurements during SOLVE/THESEO 2000, *J. Geophys. Res.*, *107*(D20), 8294, doi:10.1029/2001JD001125.
- Jiang, J. H., S. D. Eckermann, D. L. Wu, and J. Ma (2004), A search for mountain waves in MLS stratospheric limb radiance from the Northern Hemisphere: Data analysis and global mountain wave modeling, *J. Geophys. Res.*, *109*(D3), D03107, doi:10.1029/2003JD003974.
- Knopf, D. A., T. Koop, B. P. Luo, U. G. Weers, and T. Peter (2002), Homogeneous nucleation of NAD and NAT in liquid stratospheric aerosols: Insufficient to explain denitrification, *Atmos. Chem. Phys.*, *2*, 207–214.
- Kondo, Y., H. Irie, M. Koike, and G. E. Bodeker (2000), Denitrification and nitric acid in the Arctic stratosphere during the winter of 1996–1997, *Geophys. Res. Lett.*, *27*, 337–340.
- Koop, T., B. P. Luo, A. Tsias, and T. Peter (2000), Water activity as the determinant for homogeneous ice nucleation in aqueous solutions, *Nature*, *406*, 611–614.
- Luo, B. P., C. Voigt, S. Fueglistaler, and T. Peter (2003), Extreme NAT supersaturations in mountain wave ice PSCs: A clue to NAT formation, *J. Geophys. Res.*, *108*(D15), 4441, doi:10.1029/2002JD003104.
- Mann, G. W., S. Davies, K. S. Carslaw, M. P. Chipperfield, and J. Kettleborough (2002), Polar vortex concentricity as a controlling factor in Arctic denitrification, *J. Geophys. Res.*, *107*(D22), 4663, doi:10.1029/2002JD002102.
- Mann, G. W., S. Davies, K. S. Carslaw, and M. P. Chipperfield (2003), Factors controlling Arctic denitrification in cold winters of the 1990s, *Atmos. Chem. Phys.*, *3*, 403–416.
- Northway, M. J., *et al.* (2002), An analysis of large HNO<sub>3</sub>-containing particles sampled in the Arctic stratosphere during the winter of 1999–2000, *J. Geophys. Res.*, *107*(D20), 8298, doi:10.1029/2001JD001079.
- Pagan, K. L., A. Tabazadeh, K. Drdla, M. E. Hervig, S. D. Eckermann, E. V. Browell, M. J. Legg, and P. G. Foschi (2004), Observational evidence against mountain-wave generation of ice nuclei as a prerequisite for the formation of three NAT PSCs observed in the Arctic in early December 1999, *J. Geophys. Res.*, *109*, D04312, doi:10.1029/2003JD003846.
- Pierce, R. B., *et al.* (2003), Large-scale chemical evolution of the Arctic vortex during the 1999/2000 winter: HALOE/POAM III Lagrangian photochemical modeling for the SAGE III—Ozone Loss and Validation Experiment (SOLVE) campaign, *J. Geophys. Res.*, *108*(D5), 8317, doi:10.1029/2001JD001063.
- Popp, P. J., *et al.* (2001), Severe and extensive denitrification in the 1999–2000 Arctic winter stratosphere, *Geophys. Res. Lett.*, *28*, 2875–2878.
- Prather, M. J. (1986), Numerical advection by conservation of second-order moments, *J. Geophys. Res.*, *91*(D6), 6671–6681.
- Santee, M. L., G. L. Manney, N. J. Livesey, and J. W. Waters (2000), UARS Microwave Limb Sounder observations of denitrification and ozone loss in the 2000 Arctic late winter, *Geophys. Res. Lett.*, *27*(19), 3213–3216.
- Shine, K. P. (1987), The middle atmosphere in the absence of dynamical heat fluxes, *Q. J. R. Meteorol. Soc.*, *113*, 603–633.
- Tabazadeh, A. (2003), Commentary on “Homogeneous nucleation of NAD and NAT in liquid stratospheric aerosols: Insufficient to explain denitrification” by Knopf *et al.*, *Atmos. Chem. Phys.*, *3*, 863–865.
- Toon, O. B., A. Tabazadeh, E. V. Browell, and J. Jordan (2000), Analysis of lidar observations of Arctic polar stratospheric clouds during January 1989, *J. Geophys. Res.*, *105*(D16), 20,589–20,615.
- Voigt, C., *et al.* (2003), In situ mountain-wave polar stratospheric cloud measurements: Implications for nitric acid trihydrate formation, *J. Geophys. Res.*, *108*(D5), 8331, doi:10.1029/2001JD001185.
- Waibel, A. E., T. Peter, K. S. Carslaw, H. Oelhaf, G. Wetzel, P. J. Crutzen, U. Poschl, A. Tsias, E. Reimer, and H. Fischer (1999), Arctic ozone loss due to denitrification, *Science*, *283*, 2064–2069.
- Wirth, M., A. Tsias, A. Dornbrack, V. Weiss, K. S. Carslaw, M. Leutbecher, W. Renger, H. Volkert, and T. Peter (1999), Model-guided Lagrangian observation and simulation of mountain polar stratospheric clouds, *J. Geophys. Res.*, *104*(D19), 23,971–23,981.

K. S. Carslaw, M. P. Chipperfield, S. Davies, and G. W. Mann, Institute for Atmospheric Science, School of the Environment, University of Leeds, Leeds LS2 9JT, UK. (gmann@env.leeds.ac.uk)

S. Eckermann, Middle Atmospheric Dynamics Section, Code 7646, E. O. Hulburt Center for Space Research, Naval Research Laboratory, Washington, DC 20375-5320, USA.